ERICA tiltrotor airframe wake characterization

Fabrizio De Gregorio*, Daniel Steiling, Ernesto Benini***, Rita Ponza******

*** Italian Aerospace Research Centre (CIRA), Italy**
****RUAG Aviation, Switzerland**
***** Padova University, Italy**
****** HIT09, Italy**

Keywords: **Tiltrotor, Aerodynamic Optimization**, **Drag Reduction**, **WT test campaign, S-PIV, Wake Characterization, CFD.**

Abstract

In the framework of the European JTI CleanSky GRC2 project devoted to drag reduction of airframe and non-lifting rotating systems of the Green Rotorcraft ITD, a CFD-based optimization was performed on the ERICA tiltrotor configuration and validated by wind tunnel tests. Previous work dealt with the shape optimization of different parts of the tiltrotor fuselage (nose, sponsons, wing/fuselage fairings, empennages) for drag reduction and efficiency improvement purposes, using CFD coupled with innovative design methodologies based on multi-objective evolutionary algorithms. In this paper, a characterization of the ERICA tiltrotor aft fuselage wake is presented based on experimental stereo PIV and numerical investigations. The flow structures are analyzed in relation to the drag reduction observed for the optimized sponsons in comparison to the baseline configuration.

1. INTRODUCTION

The peculiar characteristic of the tilt-rotor is the capability to take-off and land like a helicopter and at the same time to cruise like an airplane. This is achieved by tilting the rotor nacelles perpendicular to the flight direction, in helicopter mode, or parallel to the flight direction, in aircraft mode. The most recent tiltrotor concepts (such as the European civil tiltrotor ERICA [1]) share some advantageous features of the traditional tiltrotors with the tilt-wing aircraft, i.e. the capability of tilting the outboard portions of the wings independently from the proprotor. This configuration removes the loss of thrust due to the downwash of the rotors on the wings in helicopter mode, giving the opportunity to reduce the rotor dimensions and thus improve cruise performance. Moreover, the smaller dimensions of the rotors gives the tiltrotor like ERICA STOL (Short Take-Off and Landing) capabilities, meaning that take-off and landing in airplane mode are possible. An aerodynamic optimization in terms of drag increases flight speed, operational range, load capability, reduces the fuel consumption and consequently the environmental impact and enhances the economic appeal of the new concept. While tiltrotors operate under a wide range of flight conditions, from hover to cruise passing through several intermediate states, the primary focus for aircraft performance optimisation lies on the cruise phase. In cruise, tiltrotors can be likened to conventional transport aircrafts, regional turboprop aircrafts in particular. The typical drag breakdown of a generic transport aircraft [2] is illustrated in Fig. 1. Viscous and lift induced drag contribute by approximately 85% to the total value. The next largest contribution, with 10%, is due to the afterbody wake shedding and the resulting pressure drag. The remaining contributions stem from aerodynamic interference phenomena, roughness, leakage and shock wave drag. This last contribution can be neglected for the tiltrotors due to the low cruise speed.

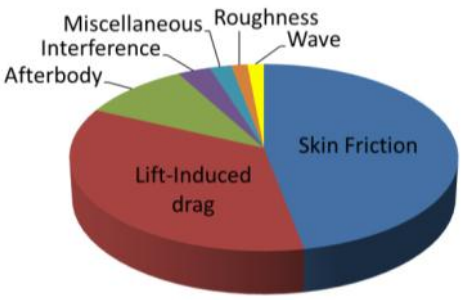

Fig. 1. Transport aircraft Drag Breakdown

In the recent past, in order to evaluate the drag build-up of the ERICA airframe and its rotating

non-lifting components, a wind tunnel test campaign was carried out with a non-motorised scaled model [**3**]. The result (Fig. 2) shows that the fuselage, the wing/fuselage fairings, the sponsons, the fin and tail plane represent about 50% of the total measured body-induced drag.

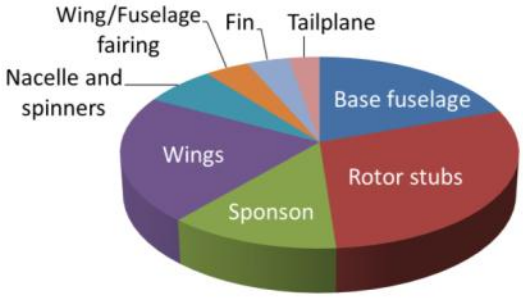

Fig. 2. ERICA Body induced drag Breakdown

Therefore, a considerable reduction in power requirement is expected to be achievable by increasing the aerodynamic efficiency of the tiltrotor airframe and the rotating non-lifting components.

In the framework of the CleanSky sub-project GRC2 “Drag reduction of airframe and non-lifting rotating systems” of the Green Rotorcraft ITD, a CFD-based optimization activity has been carried out, resulting in optimised shapes of the tiltrotor fuselage [4]. In particular, the shape of the nose, sponsons, wing/fuselage fairings and empennages were altered using CFD coupled with an innovative design methodology based on evolutionary algorithms [5][6]. A subsequent wind tunnel test campaign with a 1:8 scale unpowered model with fixed stub rotors (Fig. 3), in the framework of the DREAm-TILT project [**7**], allowed to assess and validate the CFD results. The aerodynamic performance of the ERICA baseline was compared to the optimised components and the singular and global benefit in terms of efficiency and in particular drag reduction were evaluated.

In addition to the global force measurements, and for a limited number of cases, the wake downstream of the landing gear sponsons was measured by Stereo Particle Image Velocimetry technique (S-PIV). The three velocity components of the flow field thus obtained provide a localised validation of the CFD tools adopted in the optimization phase. These wake flow measurements were carried out to better understand the flow mechanism responsible for the benefits observed for the new optimised sponsons. The evaluation of the aerodynamic benefit of the optimised sponsons compared to the baseline configuration and the wake behaviour is the main objective of this work. In the following, the experimental and CFD tools selected for the investigation of the optimised and original sponsons configuration are discussed. The collected data, the experimental and numerical comparison and the drag reduction are presented in terms of global loads as well as of flow field behaviour.

Fig. 3. ERICA model in RUAG LWTE Test Section – Front View

2. EXPERIMENTAL LAYOUT

2.1. Test facility and model description

The test campaign with a 1:8 scale model of the ERICA tiltrotor configuration was performed in the RUAG LWTE wind tunnel. The LWTE is an atmospheric closed loop wind tunnel, with a cross section of 7 x 5 m. A wind speed of V=50 m/s was selected for the tests, corresponding to a Reynolds number based on the mean aerodynamic chord of approximately Re=930.000. The model parts included the new optimised geometries: nose, wing/fuselage fairing, sponsons, and empennage. The model was not powered and the rotor blades were replaced by fixed stubs. The model’s main dimensions are:

- wing span (bw): 1.875 m
- mean aerodynamic chord (cwmac):0.3038 m
- fuselage length (L): 2.1 m
- wing surface (Sw): 0.578 m^2

The modular model build-up allowed the investigation of the singular influence of the different optimized components on the aerodynamic loads. For the flow field measurements, the model is mounted in the up-right position without the vertical fin and supported by the dorsal strut. This setup is chosen to minimize disturbances in the regions of interest (sponsons).

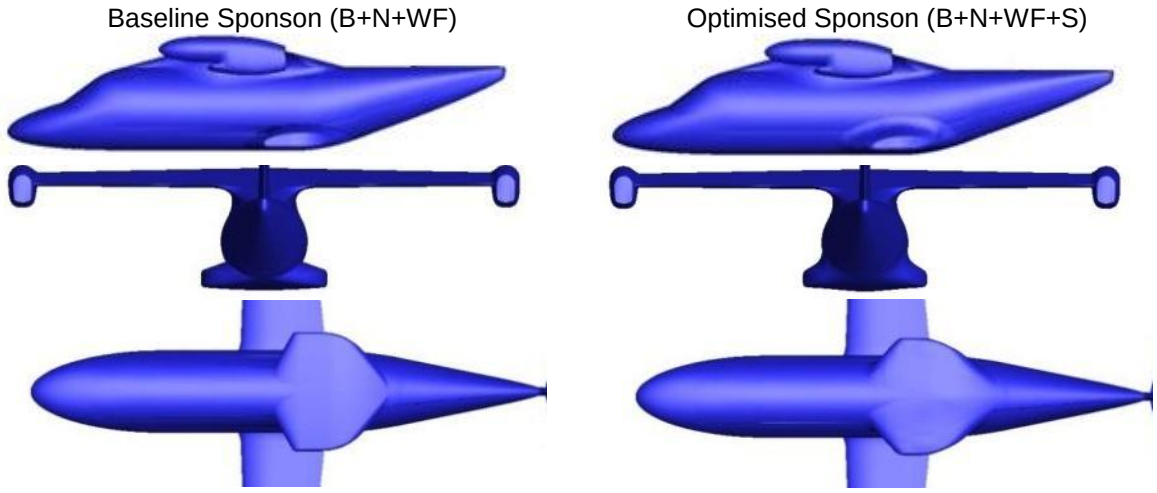

Fig. 4. Baseline and Optimised sponsons surface

2.2. Instrumentation and Data Acquisition

The aerodynamic forces an moments acting on the wind tunnel model were acquired with an internal six component balance (RUAG 192). The static accuracy of this type of balance is in the order of 0.1% of the design loads for all components and load combinations over the entire measurement range. Even more important than accuracy of the absolute measurement values is the repeatability of the test. Based on theoretical considerations, a repeatability of approximately 3 drag counts was expected for the full measurement chain. This value was later confirmed during the wind tunnel test.

Secondary instrumentation included, amongst other sensors, Schaevitz LSRP inclinometers with an accuracy of 0.03° for recording the actual pitch and roll attitude of the wind tunnel model.

Different corrections have been applied to the wind tunnel data. The effects of blockage and flow angularity have been corrected using a wall pressure signature method [8]. Strut interference effects due to the ventral strut have been determined and corrected using measurements with a ventral dummy strut while the model was mounted on the dorsal strut.

2.3. Flow field measurements

The flow field characteristics downstream of the fuselage sponsons were investigated by stereo PIV measurements. The measurements were carried out at four different vertical cross planes at different distances from the model nose (x/L=0.74, 0.79, 0.83, and 0.93) and respectively named PIV1, PIV2, PIV3 and PIV4. An additional plane PIV5 at x/L=0.88 was measured for the baseline configuration only. The measurement planes for both model configurations are shown in Fig. 5.

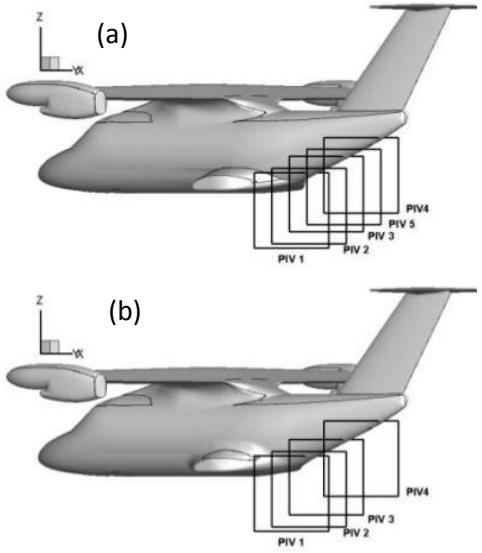

Fig. 5. PIV recording region: Baseline Sponsons (a) and Optimised Sponsons (b).

The PIV system was composed of two Nd-Yag resonator heads providing a laser beam of about 250 mJ each at 532 nm and by two double frame CCD cameras (2048x2048 px). Particles of about 1 μm of diameter, composed of DEHS oil, were used as seeding. The seeding was injected downstream of the test section in order to obtain uniform seeding concentration of the full circuit. The laser was located under the test section. The laser light sheet was projected upward into the test section trough an acrylic window installed in the test section floor. The light sheet optics were mounted on a linear traversing system remotely controlled in order to translate the light sheet along the wind tunnel longitudinal axis. Each

recording camera was mounted on a 2D linear traversing system and located outside of the test section, inside the door frames of the side wall rear doors, downstream of the model. The traversing systems allowed to rigidly translate the cameras and light sheet plane without the need for additional calibrations of the stereo set up, thus increasing significantly the measurement productivity. Each camera was equipped with a motorised Scheimpflug support, 200 mm Canon EOS lens and lens remote control. The viewing angle between the stereo cameras was about 96°, close to the optimum values of 90°. The stereo lay-out is illustrated in Fig. 6.

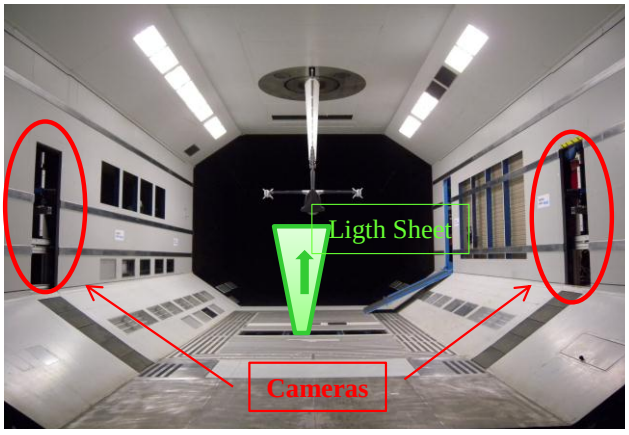

Fig. 6. Recording lay-out in RUAG LWTE TS

The stereo PIV cameras recorded a field of view of 500x346 mm^2 providing a velocity vector spatial resolution of about 4.5 mm/vector. The test matrix foresaw testing at a constant WT speed of V=50m/s, two model configurations, model incidence angles varying from -6° to +2° with a step of α=2° and an additional point at α=10°, yaw angles ranging from -5° to +5° with an angle step of β=5° and S-PIV measurements on five parallel planes for a total number of 66 test cases.

3. CFD code description

An extensive numerical simulation campaign was carried out for the baseline and optimized configurations of the 1/8 scaled tiltrotor fuselage. The support system was included in the numerical model either in the ventral or dorsal mode, depending on the test case, in accord with the experimental test matrix carried out in the RUAG wind tunnel. For each geometrical configuration, the aircraft pitch attitude was varied from -18° to 18°. In addition, a limited number of simulations at non-zero sideslip angles were carried out (yaw attitude was varied from 0° to 10°). The wind tunnel model was created using the actual LWTE cross-section shape and size, while along the longitudinal direction the length was established based on previous experience that suggests an extension of the fluid domain 2÷3 aircraft lengths upstream and 5÷6 lengths downstream of the fuselage. A view of the model inserted in the wind tunnel is show in Fig. 7.

The numerical mesh was built up using Hypermesh® and it was of the hybrid type: prismatic layers were created over the aircraft and pylons surfaces in order to better resolve the boundary layer, while tetrahedral elements were used in the rest of the fluid domain. The overall mesh size was 16.2 M elements (on one half aircraft).

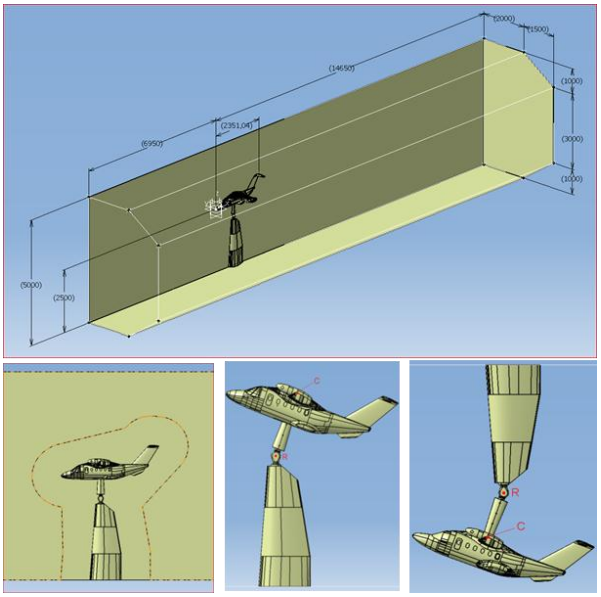

Fig. 7. ERICA model inside the wind tunnel with both ventral and dorsal struts.

Ansys Fluent® was used as the CFD solver: steady simulations were carried out, using k-ω SST turbulence modeling with specification of turbulent intensity and hydraulic diameter.

3.1. Optimization methodology

The optimization procedure used in CODE-tilt for identifying the optimal shapes of the tiltrotor fuselage components is structured in three phases:

1) Baseline model preparation and simulation phase;
2) Automatic optimization phase;
3) Post-processing.

3.1.1. Baseline model simulation

Typically the starting point is represented by the CAD model of the baseline configuration (Dassault Systemes CATIA® V5 was chosen for the present application). Starting from the geometrical model, the procedure moves into the "baseline simulation block" [9], where the baseline configuration of the component under consideration is analyzed, in terms of aerodynamic performance in the most relevant operating conditions, via CFD computation using the selected flow solver. The assessment of the baseline solution allows the designer to properly understand the flow field characteristics of the object under analysis. Specifically, it gives fundamental indications for the optimization objectives and constraints identification and allows to properly set up the geometrical parametric model.

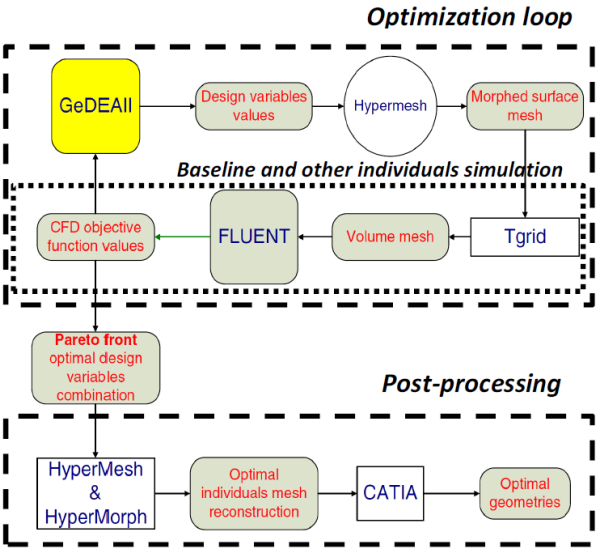

Fig. 8. Optimization method flow-chart.

3.1.2. Automatic optimization execution

Once the preliminary operations are completed, the automatic optimization loop starts (Fig.8): the procedure is made up by the following components:

1) GDEA (Genetic Diversity Evolutionary Algorithm): it is an advanced multi-objective optimization algorithm based on evolutionary techniques developed at the University of Padova [9] and it acts as the optimization engine;

2) Altair HyperMorph®: it allows the conversion of design parameters selected by GDEA into morphed CFD cases, suitable for objective function evaluation;

3) Ansys Fluent®: the selected flow solver; it takes as an input the morphed CFD cases coming from HyperMorph® and gives back to GDEA the correspondent values of the selected objective functions.

During the optimization process, GDEA lets a population of individuals (each one corresponding to a different set of design variables and so to a different geometry configuration) "evolve" until the convergence to the Pareto optimal frontier has been reached. The Pareto frontier represents the solution of a multi-objective optimization problem, and is made up of a set of so-called "non-dominated" solutions. A non-dominated solution is one in which an improvement in one of the objectives necessarily requires the degradation of another [10].

3.1.3.Post-processing

The Pareto frontier, which is the output of the automatic optimization loop, represents a multiple set of solutions equally optimal according to the Pareto concept, but of course different from the aerodynamic and engineering point of view. Indeed, each solution over the Pareto frontier may present advantages and drawbacks with respect to the other solutions. In order to identify, among the optimal set, the most appropriate design, a post-processing activity is necessary. Thanks to the intrinsic multi-objective approach adopted, the designer is allowed to select, among the Pareto optimal set, the solution which is most suitable for his/her needs: for example, choosing to privilege the improvement of one objective with respect to another or even including other considerations such as non-aerodynamic requirements. The strength of the selected approach is that the designer can choose the proper trade-off between the objectives when the optimization work has been completed and he is not forced to introduce his arbitrariness in the problem set up, as commonly happens using traditional optimization approaches.

4. Results

4.1. Repeatability Assessment

The flow velocity measurement part of the test campaign was carried out at the end of the main test campaign, which focused on the aerodynamic loads characterization. The accurate and repeatable setting of the test condition was one of the main considerations during the PIV test campaign. The accuracy can be verified by

comparing the aerodynamic coefficients acquired during the PIV measurements with the data of the previous loads test campaign. The lift and drag coefficients comparison demonstrates a good repeatability of the test conditions. As an example, the lift and drag coefficients for the baseline model at β=0° are shown in Fig. 9 and Fig. 10. The continuous line indicates the result of the polar sweep whereas the data obtained during the stationary PIV measurements are indicated by the markers. The dispersion is found to be in the range of 0.5to 1lift count (0.01 of lift coefficient, Fig. 9) and 7 (up to 15 in some cases) drag counts (0.0001 of drag coefficient, Fig. 10). The observed dispersion is within expectancies (combined repeatability of the wind tunnel measurement chain and the wind tunnel model itself) and is found to be satisfactory for the assessment of the flow field.

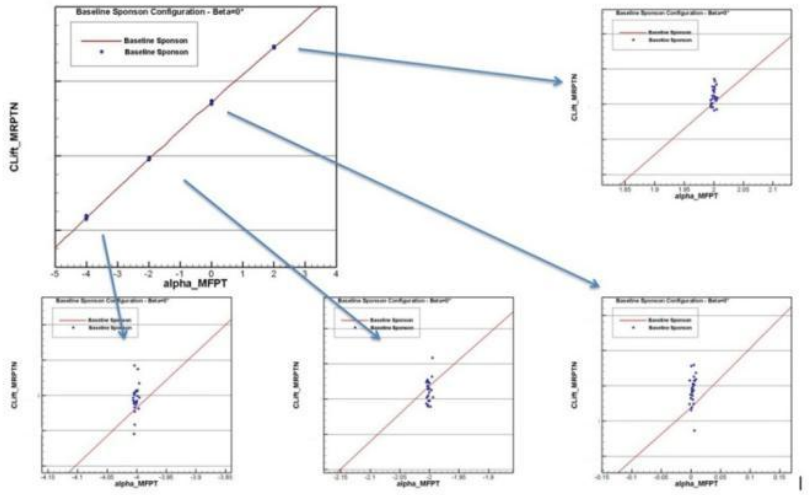

Fig. 9 Baseline sponson – Lift Coefficient Repeatability Test α=0° and β=0°

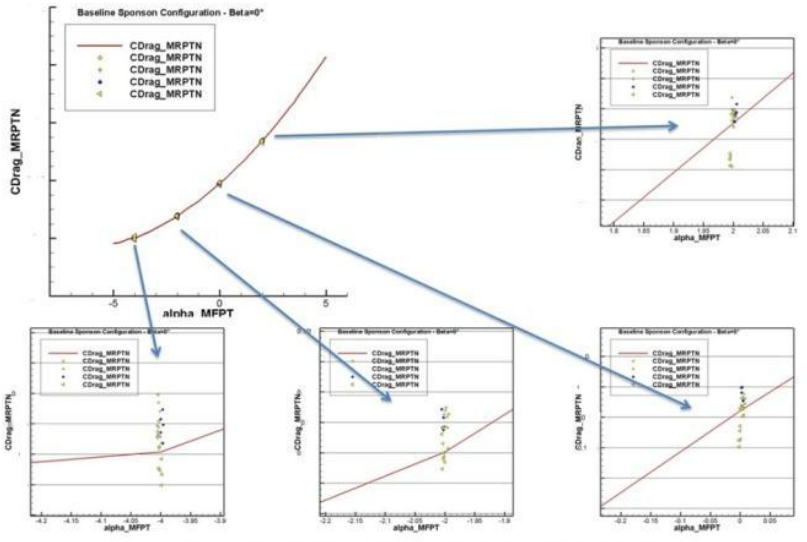

Fig. 10 Baseline sponson – Drag Coefficient Repeatability Test α=0° and β=0°

4.2. Aerodynamic load measurements

The experimental assessment of the fuselage geometry optimization in terms of drag reduction was the main scope of the DREAm-TILT project. Hereafter, the experimental and numerical results obtained on the full model configuration for the baseline and optimised sponsons are presented (Fig. 11). The experimental results are shown with continuous coloured lines whereas the CFD results are plotted as coloured markers.

The comparison of the optimised sponsons versus the baseline sponsons for a sweep polar in the range between α=-5° and α=+5° shows a fairly identical behaviour of the lift coefficient except for an almost negligible reduction of the lift slope (Fig. 11 a), a clear benefit in terms of drag reduction in

the range between 15 to 30 drag counts (Fig. 11 b) and similar pitching moment trends with a small reduction of the longitudinal stability indicated by a reduction of the negative slope (Fig. 11 c). The efficiency of the optimised configuration is thus clearly improved: at the same lift coefficient the drag is reduced (Fig. 11 d).

The CFD results show the same trends as the experimental data. The lift slope decreases, the drag reduction and pitching moment slope reduction are clearly detected. The quantitative results show a remarkable agreement between the experiment and the numerical simulation for the lift and drag coefficients. The drag values in the range between α=-5° and α=0° show differences smaller than 1%. For other incidence angles, the worst case is smaller than 4%. The difference can best be explained by the complex interaction of the dorsal strut wake with the flow over the ERICA wing, especially at higher lift coefficients. For cases with a ventral strut, the correlation between CFD and experiment is better, even at higher lift coefficients.

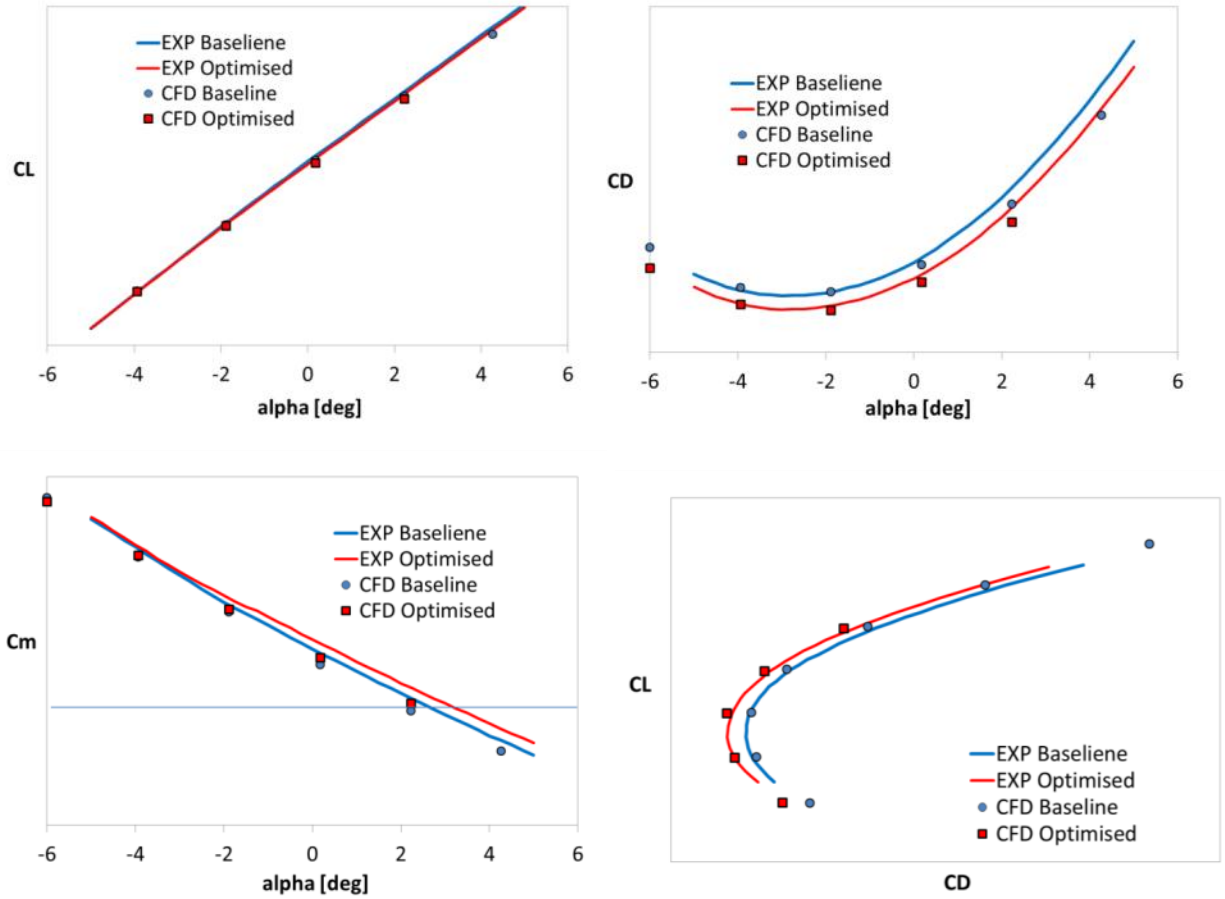

Fig. 11. Optimised/Baseline sponsons configuration comparison. CL and CD vs α

4.3. Flow Field measurements

The flow field measurements were aimed at investigating and comparing the flow characteristics of the wake behind the ERICA baseline sponsons and the new optimised geometry. The lower region of the Tiltrotor fuselage and in particular the region downstream of the sponsons was of interest. This region typically is responsible for the aft body drag component induced by flow separation and counter rotating vortex shedding. The flow velocity field was investigated at varying incidence angles between α=+2° to α=- 4° with angular steps of 2° and a few cases for α=+10° and -6° at zero yaw angle β=0°. An example of the wake measurement results in relation to the model geometry is shown in Fig. 12. The colour map shows out of plane vorticity. The model attitude is α=+2° and β=0°.

The wake behind the improved sponsons was studied for the same test conditions except that the measurement plane located at x/L=0.88 had to be omitted due to wind tunnel time constraints. The velocity magnitude colour map together with

the in plane velocity vectors clearly displays the flow macro structures shedding from the aircraft sponsons and fuselage (Fig.13).

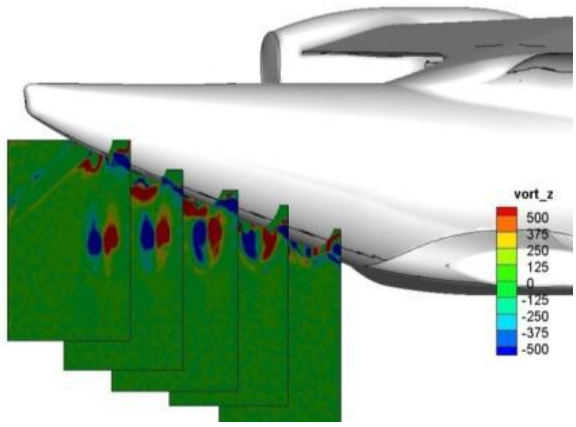

Fig. 12. Out of plane vorticity field

The results are presented as a comparison between the velocity magnitude colour plots measured on the baseline sponson model configuration at the different cross planes (upper row results in Fig. 13) and the results obtained on the improved sponsons configuration (lower row results in Fig. 13).

The case characterised by α=+2° and β=0° shows, for the baseline configuration and on the first measurement plane x/L=0.74, the development of a small symmetric wake in the proximity of the fuselage bottom. The wake then moves downstream along the fuselage, increasing in size until it detaches from the fuselage at x/L=0.83.. The flow field induced by the new optimised sponsons presents a similar behaviour but is characterised by: a smaller wake size, reduced momentum loss, delayed separation and is remaining closer to the model. A similar behaviour was found in the CFD simulation (Fig. 14). The wake released by the optimised sponsons (lower row velocity fields in Fig. 14) compared to the baseline case (upper row velocity fields in Fig. 14), has a smaller size, a delay in the wake development and a later separation from the fuselage body. Comparing the CFD results with the experimental data, in addition to the above described commonalities, some differences can be observed. The CFD velocity field predicts an earlier wake formation. The detached flow shape is almost elliptical and the connecting zone with the fuselage body is thinner.

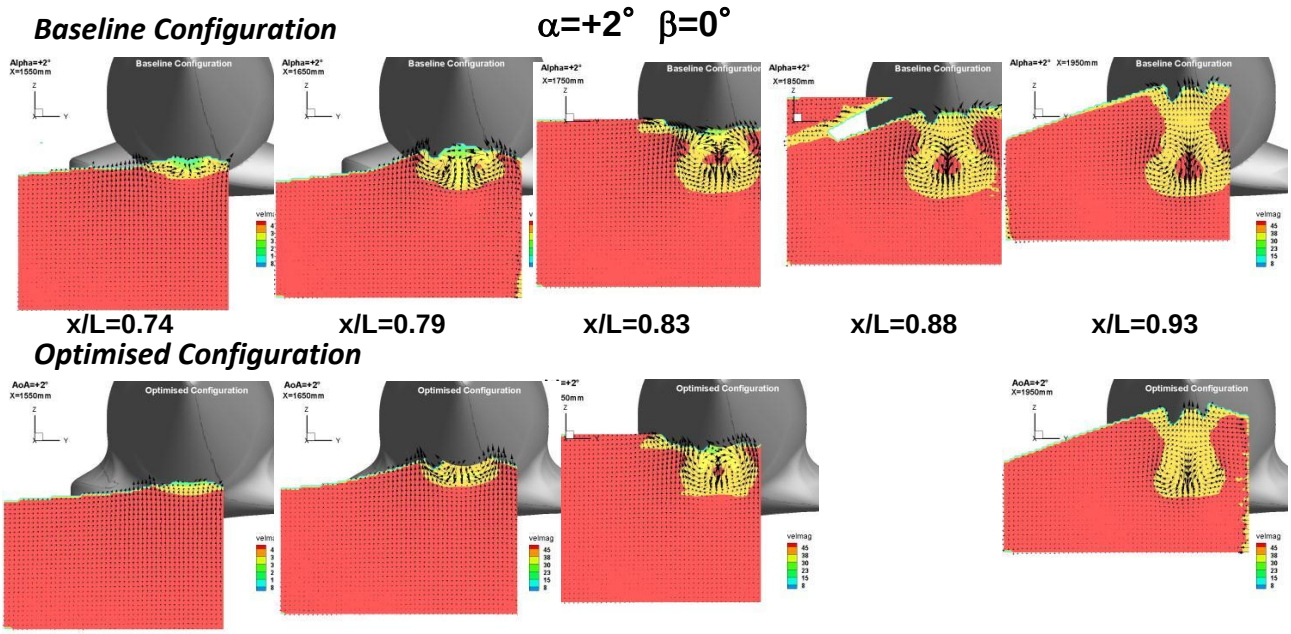

Fig. 13. PIV Velocity vector field with velocity magnitude colour map at α=+2° and β=0°

CFD Baseline Configuration **α=+2° β=0°**

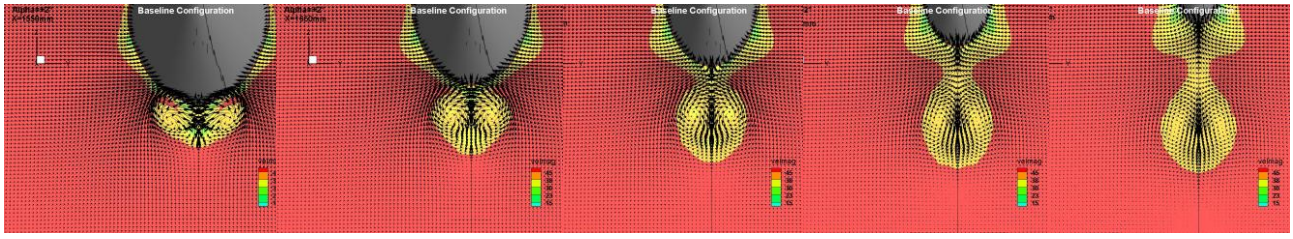

CFD optimised Configuration

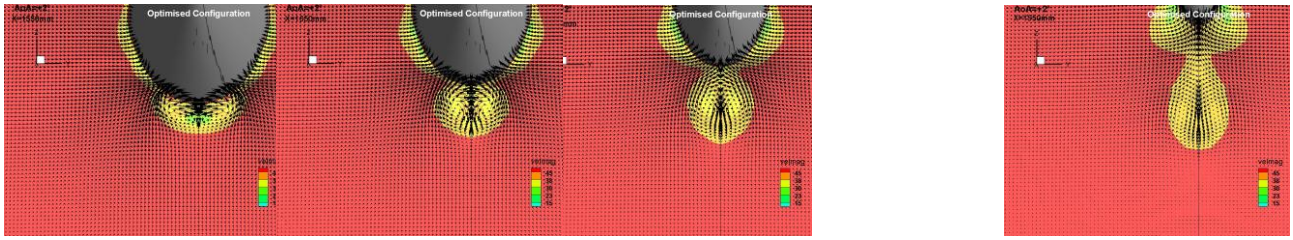

Fig. 14: CFD Velocity vector field with velocity magnitude colour map at α=+2° and β=0°

The first main difference can be explained partially by the non-availability of velocity measurements in the close proximity of the fuselage due to laser reflections. But this is not sufficient to fully justify the difference to the anticipated wake development from CFD data. The last two dissimilarities can be attributed to the unsteadiness of the wake and by the different nature of the compared data. The CFD data is the results of a RANS flow simulation with the assumption of steady flow whereas the PIV mean velocity field is obtained by averaging 150 instantaneous velocity fields. The instantaneous velocity fields induce a smoother and larger flow structure in the averaged field. This difference may be eliminated by performing transient CFD simulations and comparing similarly averaged quantities.

Baseline Configuration **α=+2° β=0°**

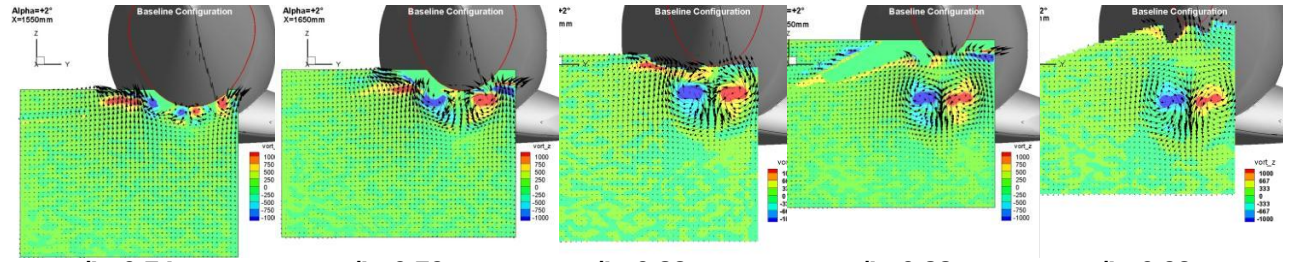

Optimised Configuration

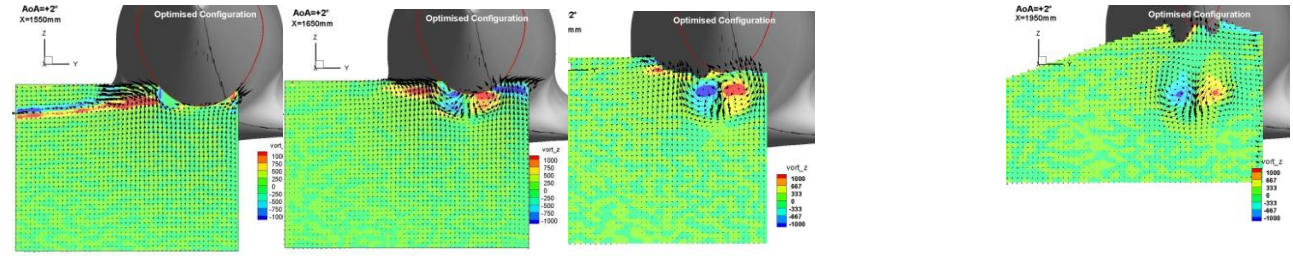

Fig. 15. Out of plane vorticity colour map at α=+2° and β=0°

Interesting conclusions can be drawn from analyzing the flow field out of plane vorticity. In figure 15, for the same case as discussed above (α=+2° and β=0°), baseline model configuration at x/L=0.74, a weak trace of the presence of two counter rotating vortices can be observed. The

vortices are clearly detectable in proximity of the fuselage at x/L=0.79 and fully developed at x/L=0.83 but still remain in the proximity of the fuselage. The real vortex detachment is evident at x/L=0.88 and the vortex cores are moving further apart at x/L=0.93. The vortex intensities increase from x/L=0.79 to 0.83 and later decrease when fully detached. This vortex behaviour is explained by the fact that up to x/L=0.83 the vortices are still connected to the fuselage and energised by the flow around the fuselage. Once the vortices are fully separated, they are exposed to dissipation phenomena. The related case for the optimised sponsons indicates at x/L=0.74 a fairly attached flow, the counter rotating vortices start to occur on the fuselage bottom at x/L=0.79 and are fully developed in the proximity of the fuselage at x/L=0.83. The vortices separate from the fuselage at x/L=0.93. The vortex intensity along the fuselage length is similar to the baseline case: the vorticity increases during the vortex growth and later decreases as the vortices separate from the fuselage. Compared to the baseline configuration, the vortical structures are of a smaller size and the vortex intensity is reduced in the order of 20-25%. They also remain closer to the surface and could induce stronger tangential velocity resulting in stronger negative pressure.

For the sake of brevity only a small number of CFD results are shown in terms of out of plane vorticity. The optimized configuration has smaller out of plane vortex intensities compared to the baseline, which agrees well with the experimental results. In comparison to the PIV results, the CFD vortex positions are further away from the fuselage (Fig. 16) and the intensities are smaller by about the 45%.

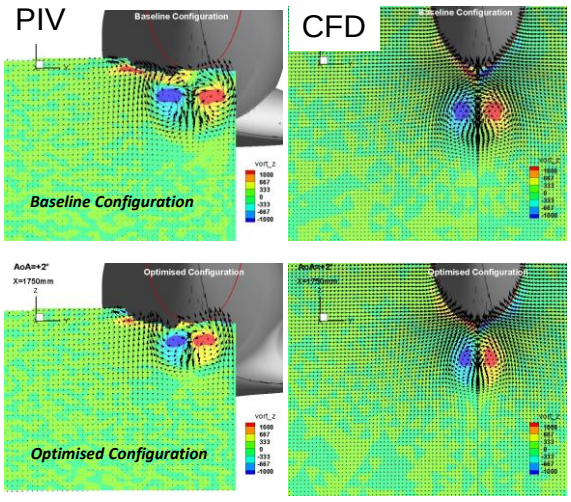

Fig. 16: PIV/CFD Vorticity colour map at x/L=0.83

The quantitative comparison of the out of plane vorticity extracted along horizontal axes passing through the vorticity peaks of the contra rotating vortices for the baseline and the optimized configuration, for the ensemble average PIV and CFD data are shown in Fig. 17. The CFD data indicates smaller vortex intensity respect the already smoothed PIV averaged data, indicating that additional unsteady simulations are necessary. In terms of global drag, the CFD out of plane vorticity underestimation provides a smaller contribution to the after body drag but is compensated by the overestimation due to the earlier wake formation (previously discussed) providing a remarkable agreement with the load data.

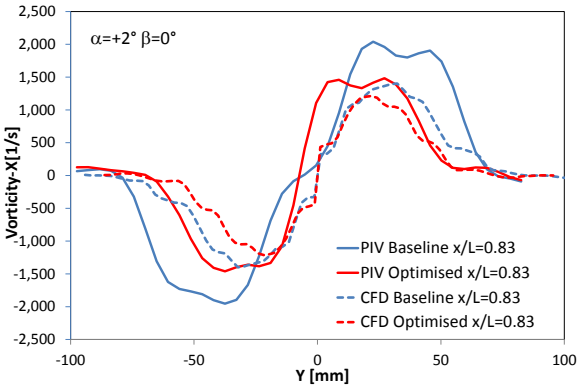

Fig. 17: PIV/CFD vorticity comparison at x/L=0.83

5. Conclusion and future activities

A test campaign has been successfully performed at the RUAG LWTE wind tunnel with the goal to investigate the wake released by the baseline and optimised sponsons for the ERICA model.. The experimental validation of the multi-objective CFD optimization procedure was successful, with good agreement of the global aerodynamic loads and the improvements in terms of drag reduction. The optimised sponsons show a drag reduction in the range between 15 to 30 drag counts, compared to the baseline configuration. For some configurations, the steady CFD simulations were in remarkable agreement with the measured aerodynamic loads. Differences encountered in the wake of some configurations were attributed to the unsteadiness of the flow, which would require time resolved CFD simulations for better comparisons.

The S-PIV wake characterization has been performed at constant flow speed for different fuselage attitude and yawing angles. The chosen S-PIV experimental set-up gave a high level of

measurement productivity, resulting in data for a large amount of test conditions.

The measured velocity fields showed a couple of contra rotating vortices shedding downstream of the fuselage sponsons. From the PIV and CFD data the following conclusions can be drawn:

1. The flow field measurements indicate a clear wake reduction in terms of size and momentum loss, of the order of about 2% of the flow rate ratio. Furthermore the vortex shedding for the optimised sponsons is delayed compared to the baseline, and the wake remains closer to the fuselage body.
2. The out of plane vorticity showed a notable intensity reduction by about 20% to 35% for the optimised sponsons in comparison to the baseline configuration.
3. Considering the effect of the optimised configuration with respect to the baseline, the CFD and the PIV results were similar showing size and vorticity alleviation.
4. A direct CFD and PIV data comparison shows some differences. The wake presents an earlier formation for the CFD results respect to the PIV data. The CFD wake shape is almost elliptical against a less uniform PIV profile. The CFD vortex intensity is smaller of about the 40% respect to the PIV data.
5. The vortex development for the different model attitudes has been measured and vortex growth and the dissipation phenomena can be investigated.
6. A valuable contribution to the experimental data base has been generated with the flow field measurements for future comparison with CFD simulations.

Additional CFD simulations are foreseen in order to take into account the unsteadiness of the flow field and to allow better comparisons with the experimental data. This will help to further validate the CFD model.

Acknowledgment

The research activities presented throughout this paper have been partially funded by the European Community's Seventh Framework Program (FP/2007-2013) for the Clean Sky Joint Technology Initiative under grant agreement number: CSJU-GAM-GRC-2008-01. The authors would like to thank the Clean Sky Joint Undertaking for the financial and managing support. The authors would like to acknowledge Dr. Jürg Müller and the LWTE crew for the valuable support provided during the measurement campaign.

References

[1] Nannoni, F., Giancamilli G., and Cicalè M., 2001, ERICA: the european advanced tiltrotor, in Proceeding of the 27th European Rotorcraft Forum, pp. 55.1–55.15

[2] Thomas A.S.W., Aircraft Drag Reduction Tecnology – A summary, AGARD R 723, pp 1.1 – 1.20, July 1985.

[3] Campanardi G., Zanotti A., Macchi C., (2008) Final complete wind tunnel test database. technical report. Technical report, NICETRIP/POLIMI/WP4.TR007/4.0

[4] Benini E., and Ponza R., CODE-Tilt Proposal. JTI-CS-2010-1-GRC-02-004.

[5] Garavello A., Benini E., Ponza R., Multi-Objective Aerodynamic Design of Tilt-Rotor Airframe Components by Means of Genetic Algorithms and CFD (TILTOp, CODETILT). Proc 68th AHS international annual forum, Fort-Worth, Texas, USA, pp511-526, 1-3 May 2012.

[6] Comis Da Ronco C., Ponza R., Benini E., Aerodynamic Shape Optimization in Aeronautics: A Fast and Effective Multi-Objective Approach. Archives of Computational Methods in Engineering, Volume 21, Issue 3, pp 189-271, September 2014.

[7] Ponza R., Assessment of tiltrotor fuselage drag reduction by wind tunnel tests and CFD (DREAm-TILT) Technical Proposal, GA no. 336439.

[8] Hackett J. E., Sampath S. and Phillips C. G., "Determination of wind tunnel constraint effects by a unified pressure signature method. Part 1: Applications to winged configurations," Lockheed-Georgia, Marietta, Georgia, NASA-CR-166186, 1981

[9] Toffolo A. and Benini E., Genetic diversity as an objective in multi-objective evolutionary algorithms. Evolutionary Computation, MIT press journal, 11(2):151–167, 2003.

[10] Deb K., Multi-Objective Optimization Using Evolutionary Algorithms. Wiley, 2001.